

**A Novel Mechanism for Calmodulin Dependent Inactivation of Transient
Receptor Potential Vanilloid 6**

Neil Bate, Rachel E. Caves[‡], Simon P. Skinner[†], Benjamin T. Goult[#], Jaswir Basran,
John S. Mitcheson & Geerten W. Vuister^{*}

Department of Molecular and Cell Biology, Leicester Institute of Structural and
Chemical Biology, University of Leicester
Henry Wellcome Building, Lancaster Road, Leicester, LE1 9HN, United Kingdom.

[‡]Present address:

School of Physiology, Pharmacology and Neuroscience. Faculty of Biomedical
Sciences, University of Bristol, University Walk, Bristol, BS8 1TD
United Kingdom.

[†]Present address:

School of Molecular and Cellular Biology, Faculty of Biological Sciences & Astbury
Centre for Structural Molecular Biology, University of Leeds, Leeds, LS2 9JT, United
Kingdom.

[#]Present address:

School of Biosciences, University of Kent, Canterbury, Kent, CT2 7NJ, United
Kingdom.

^{*}Corresponding author (gv29@leicester.ac.uk)

running title: Calmodulin Dependent Inactivation of TRPV6

Abstract

The paralogues TRPV5 and TRPV6 belong to the vanilloid subfamily of the Transient Receptor Potential (TRP) superfamily of ion channels and both play an important role in overall Ca^{2+} homeostasis. The functioning of the channels centres on a tightly controlled Ca^{2+} -dependent feedback mechanism where the direct binding of the universal Ca^{2+} -binding protein calmodulin (CaM) to the channel's C-terminal tail is required for channel inactivation. We have investigated this interaction at the atomic level and propose that under basal cellular $[\text{Ca}^{2+}]$ CaM is constitutively bound to the channel's C-tail via CaM C-lobe only contacts. When cytosolic $[\text{Ca}^{2+}]$ increases charging the apo CaM N-lobe with Ca^{2+} , the CaM:TRPV6 complex rearranges and the TRPV6 C-tail further engages the CaM N-lobe via a crucial interaction involving L707. In a cellular context, mutation of L707 significantly increased the rate of channel inactivation. Finally, we present a model for TRPV6 CaM-dependent inactivation, which involves a novel so-called “two-tail” mechanism whereby CaM bridges between two TRPV6 monomers resulting in closure of the channel pore.

keywords

TRPV6 calcium channel ; NMR ; ITC ; electrophysiology ; Calmodulin

Introduction

In humans, the Transient Receptor Potential (TRP)[‡] superfamily of twenty-seven ion channels are divided into six sub-groups (TRPC; TRPV; TRPM; TRPP; TRPA; TRPML). The members of the TRP superfamily have been grouped together based on proposed structural homology, such that members within each group are functionally diverse and expressed in a wide array of cell and tissue types¹. Fundamental physiological roles have been clearly established from the identification of channel dysfunction-related pathologies (channelopathies)², in addition to aberrant gene expression studies in various cancer cell types³. Recently, the structures of the transmembrane spanning parts of four distinct TRP channels have been solved; TRPV1⁴, TRPV2⁵, TRPV5⁶ and TRPA1⁷ by cryo-EM whereas TRPV6 has been solved by both X-ray crystallography⁸ and by cryo-EM⁹. These analyses confirmed the previously postulated channel topology; i.e. native channels are tetrameric with each TRP subunit consisting of six transmembrane helices. Helices five and six of each subunit are arranged within the tetramer to form the ion-conducting pore, analogous to potassium channels and an iris-like channel opening. Each transmembrane region is flanked by cytosolic N- and C-termini of varying lengths¹⁰. Moreover, the C-termini are in close proximity to the pore and surrounded by an outer skirt consisting of the N-terminal ankyrin repeats.

The epithelial Ca²⁺ channel TRPV6 is a member of the vanilloid subfamily and, together with its paralogue TRPV5, perform an important role in Ca²⁺ homeostasis¹¹. These channels are highly selective¹¹ for Ca²⁺^{12,13} and are expressed within a range of epithelial cell types^{12,14}. Unlike *Trpv5*^{-/-} null-mice, which exhibited a defect in bone formation due to excessive loss of Ca²⁺ in the urine¹⁵, *Trpv6*^{-/-} null-mice were still viable on a normal calcium diet¹⁶; however they exhibited an increase in male sterility due to a block in Ca²⁺ uptake by the epididymal epithelium¹⁶.

In order to tightly regulate Ca²⁺ entry into the cell, TRP channels engage a Ca²⁺-dependent feedback mechanism(s) to inactivate the channel (channel gating).

[‡] **Abbreviations** CaM: Calmodulin; C-tail: C-terminal tail of the TRPV6 channel; CSP: chemical shift perturbation; EM: Electron Microscopy; FRET: Foster resonance energy transfer; ITC: isothermal titration calorimetry; NMR: nuclear magnetic resonance; N-tail: N-terminal tail of the TRPV6 channel; TRP: transient receptor potential; TRPV: transient receptor potential vanilloid; HEK293: human embryonic kidney; GB1: B1 domain of protein G.

Thus, on the basis of experiments in whole HEK293 cells TRPV6 channel inactivation was proposed to occur via a fast Ca^{2+} -dependent component together with a slower CaM-dependent component^{17,18}. A number of Ca^{2+} -responsive proteins have been shown to directly interact with TRPV5 and/or TRPV6; these include Calbindin- $\text{D}_{28\text{K}}$ ¹⁹, 80-KH²⁰ and Calmodulin (CaM)²¹⁻²⁴. Peptide scanning using *in silico* predicted CaM binding sites identified five short TRPV5 peptide sequences capable of binding CaM²³⁻²⁵. Moreover, deletion of the C-terminal TRPV5 CaM binding site²⁶ or mutation of the analogous region in TRPV6¹⁸ significantly increases cellular $[\text{Ca}^{2+}]$ without altering the membrane localisation of the channels in HEK293 cells. These observations for TRPV5 and TRPV6 are in line with those observed for other TRP channels; for example, channel desensitisation has also been achieved by deletion of the membrane distal C-terminal CaM binding site in either TRPC1²⁷, TRPV1²⁸ or TRPV4²⁹. In addition, CaM has also been shown to bind to the cytosolic C-tails of TRPV2³⁰, strongly suggesting a similar mode of CaM-dependent channel inactivation within the TRPV family.

Taken together, these analyses strongly implicate the binding of CaM to the TRP C-tail as a key event in channel inactivation. CaM is a well-known ion channel regulator and has been proven to be very adaptable in its interaction with different targets^{31,32}. CaM consists of two independent globular domains, denoted as the N-lobe and the C-lobe, linked by a flexible region (Fig. S1A). Each lobe independently binds two Ca^{2+} ions; although *in vitro*, the C-lobe has a 6-fold higher affinity for free Ca^{2+} than the N-lobe³³.

To the best of our knowledge, a viable molecular mechanism for TRP channel inactivation by CaM has thus far remained elusive. Moreover, neither the EM nor the X-ray TRP channel structures provide any clues, as the relevant C-tails are missing in all of these structures either as a result of truncations used for performing the structural studies or due to the disordered nature of the N- and C-termini. Therefore, for the first time we present an experimentally-derived model which details how, in a cellular context, TRPV6 can be inactivated by CaM in response to elevated $[\text{Ca}^{2+}]$ via a novel so-called “two-tail mechanism”. Using a combined approach involving NMR spectroscopy, ITC and analytical gel filtration together with electrophysiology, we present data that show the CaM-dependent TRPV6 inactivation process to comprise of three distinct states of the CaM:channel complex. In the accompanying paper by

Bokhovchuk et al.⁵², we report on a structural and dynamical analysis of the complex of CaM with the TRPV5 paralogue representing the channel under basal Ca²⁺ conditions. We identify key residues for the inactivation process, including L707A, a point mutation that sensitises the system, causing an increased rate of channel inactivation in response to increased cellular [Ca²⁺]. We rationalise that the mechanism proposed here is potentially also applicable to other CaM-dependent inactivated TRP channels.

Materials and Methods

Plasmids

The TRPV6⁶⁵⁵⁻⁷²² region and mutants thereof, were generated by PCR and cloned into the *E. coli* protein expression vector pLEICS-46, which contains a N-terminal GB1 solubility tag, a His₆ affinity tag followed by a TEV cleavage site (Protex, Leicester University). CaM wild-type and mutants thereof, were generated by PCR and inserted into the *E. coli* protein expression vector pLEICS-01, which contains a His₆ affinity tag followed by a TEV cleavage site (Protex, Leicester University). The plasmids used in the electrophysiology studies were constructed as follows. TRPV6¹⁻⁷²⁵ and TRPV6^{1-725(L707A)} were generated by PCR and cloned into the mammalian expression vector pCINeo/IRES-eGFP²³. All constructs were sequence verified.

Protein expression and purification

Proteins were expressed in *E. coli* BL21 Star (DE3) (Novagen) and purified as previously described³⁴. Recombinant proteins were analysed by 16 % SDS-PAGE and stained using brilliant blue R-250. Protein concentration was determined at A₂₈₀ (Eppendorf BioPhotometer plus) using the respective extinction coefficient as determined by the ProtParam Tool (<http://web.expasy.org/protparam/>).

Analytical gel filtration

Recombinant CaM and TRPV6 proteins were dialysed into gel filtration buffer (20 mM Tris-Cl pH 8.0, 150 mM NaCl and 2 mM DTT). Complexes were formed in the presence of 10 mM Ca²⁺ at room temperature for 30 minutes. Analytical gel filtration chromatography was carried out using a Superdex-75 (10/300) column (GE Healthcare) pre-equilibrated and then run in gel filtration buffer.

NMR spectroscopy (sample preparation)

Recombinant CaM and TRPV6 proteins used in NMR experiments were dialysed against high-Ca²⁺ buffer (20 mM Tris-Cl pH 7.4, 50 mM KCl and 10 mM CaCl₂). All NMR samples contained 5% *v/v* D₂O.

NMR spectroscopy: experiments

Spectra were recorded at 308 K on Bruker 500 MHz AVI; 600 MHz AVIII; 600 MHz AVIII HD and 800 MHz AVII, with the 600 MHz and 800 MHz spectrometers equipped with CryoProbesTM. The binding of TRPV6 proteins to CaM was monitored by 2D ¹⁵N-¹H-HSQC experiments. Changes in the Ca²⁺ bound status of the CaM lobes was easily visualised by the presence or absence of representative CaM N- and C-lobe peaks (cf. Fig S1A).

For the assignment of ¹³C¹⁵N-CaM complexes with TRPV6⁶⁵⁵⁻⁷²², the following series of heteronuclear triple-resonance experiments were performed: 3D HNCA, HNCACB, HN(CO)CA, CBCA(CO)NH, HNCOC, which yielded backbone and C β chemical shift assignments. Data were analysed using CcpNmr AnalysisAssign⁵¹. CaM chemical shift perturbations (CSP) resulting from binding were calculated for individual atoms and averaged with the differences of their directly bonded neighbours using a 7:1 weighting for ¹H resonances *vs.* ¹⁵N resonances.

Minimal shift mapping using a nearest-peak based approach³⁵ was performed as follows. A resonance frequency amide peak table for each mutant spectrum was generated in TopSpin3.2 (Bruker). CSPs were calculated using a weighting for ¹H resonances *vs.* ¹⁵N resonances of 7:1 for all mutant spectra derived peaks relative to each assigned peak in the ¹⁵N-CaM_{WT}:TRPV6⁶⁵⁵⁻⁷²² wild-type spectra, with the lower limit taken as the minimal shift. This analysis was performed on the following ¹⁵N-CaM_{WT}:TRPV6 complex amide residues; CaM N-lobe residues 2-41; 44-47; 51-65; 67-70 and C-lobe residues 84-148. Thus, this analysis generates a lower limit for the CSP value of each of these backbone amide residues.

Isothermal Titration Calorimetry (ITC)

Recombinant CaM and TRPV6 proteins used in ITC experiments were prepared as for the NMR experiments (above). The concentration of CaM in the cell ranged from

17.4-23 μM with a 19-fold excess of TRPV6 protein in the syringe. ITC experiments were performed using a VP-ITC MicroCalorimeter. Samples were equilibrated to 25 $^{\circ}\text{C}$, then 20 serial injections of 5 μl were added at a stirring speed of 300 rpm at an interval of 4 minutes, followed by 19 serial injections of 10 μl under the same conditions. To correct for background heating effects TRPV6 protein was titrated into buffer alone. ITC data analysis was carried out using Origin 7 software using either a one or two site binding model.

Electrophysiological recordings

TRPV6 channel inactivation was determined by measuring the kinetics of TRPV6 currents using the whole-cell configuration of the patch-clamp technique. HEK293 cells were transiently transfected with pCINeo/IRES-eGFP TRPV6 using Lipofectamine 2000 (Invitrogen). After 4 hours, the transfection media was exchanged for a low Ca^{2+} DMEM culture media (to minimize inward calcium fluxes during cell culture) supplemented with 1.8 mM MgCl_2 (to replace CaCl_2 and keep total divalent cation concentration the same as standard culture media), 10 % serum, L-glutamine, penicillin and streptomycin. Cells were lifted off the plate using enzyme-free cell dissociation buffer (Invitrogen, UK). Cells were superfused with room temperature NMDG-based (0 Na^+ , 0 Ca^{2+}) extracellular solution containing 142 mM NMDG-Cl, 4 mM CsCl, 1 mM MgCl_2 , 10 mM Glucose, 5 mM HEPES, pH 7.4. Borosilicate glass patch-pipettes (2 – 4 $\text{M}\Omega$) were filled with an intracellular solution containing 100 mM Cs Aspartate, 20 mM CsCl, 4 mM Na_2ATP , 10 mM HEPES, 10 mM BAPTA, 1 mM MgCl_2 , pH 7.2. The recording chamber was grounded through an agar bridge connected to an Ag/AgCl pellet in 3 M KCl. A pipette offset was applied to correct for junction potentials prior to recording. Once whole cell access was achieved, cells were left for 2 mins for cell dialysis with pipette solution. Currents were elicited with 400 ms duration voltage clamp steps applied repetitively every 500 ms, from a holding potential of -20 mV to a step potential of -100 mV. To measure TRPV6 currents, the extracellular solution was switched to a 2 mM CaCl_2 , 140 mM NaCl-based ($\text{Ca}^{2+} + \text{Na}^+$) solution (all other components were the same as the NMDG-solution). Leak current was measured prior to the extracellular solution being exchanged for a 2 mM Ca^{2+} , NaCl based (control) solution. Currents were sampled at 5 kHz and recorded to disk for off-line analysis. TRPV6 currents were measured as

the peak current in $\text{Ca}^{2+} + \text{Na}^{+}$ solution, minus current in the NMDG solution. PClamp9 software (Molecular Devices) was used for data acquisition and current trace analysis and Prism (Graphpad) for figure preparation and statistical analysis. Experimental traces did not decay exponentially and consequently were best described by time analysis at 20, 50 and 80 % inactivation.

Results

TRPV6 is bound to the CaM_C lobe to form the resting Ca²⁺-open state

We previously targeted the cytoplasmic TRPV6 C-tail (residues 579-725) and identified the TRPV6⁶⁹¹⁻⁷¹⁶ C-tail peptide as a high-affinity CaM binder (K_d of 77 ± 18 nM) under a ~ 100 -fold excess of Ca^{2+} (high- Ca^{2+} conditions)²⁴. To investigate both the Ca^{2+} dependency and CaM-lobe specificity of the CaM:TRPV6 C-tail interaction, we selected the longest soluble TRPV6 region of 655-722²⁵. This fragment was used in conjunction with a set of previously described CaM mutants which have impaired Ca^{2+} binding properties in one or more of CaM's Ca^{2+} binding sites (Fig S1A)³⁶. In particular, we used variants which prevent either the N-lobe, the C-lobe or both lobes from binding Ca^{2+} . Following convention, these were denoted as CaM₁₂, CaM₃₄, and CaM₁₂₃₄, respectively, where the subscripts indicate the mutation of the relevant CaM Ca^{2+} -binding sites. The structural integrity of the mutant CaMs was confirmed by analysis of ¹⁵N-¹H-HSQC spectra, where changes in the Ca^{2+} bound status of the individual CaM lobes can be readily visualised by the presence of peaks corresponding to residues in each lobe (Figs S1B-I).

Analysis of the binding of TRPV6⁶⁵⁵⁻⁷²² to the various Ca^{2+} deficient CaM₁₂, CaM₃₄ and CaM₁₂₃₄ mutants under high- Ca^{2+} [10mM] conditions using analytical gel filtration and NMR spectroscopy revealed that disruption of all four Ca^{2+} binding sites in CaM (CaM₁₂₃₄) was sufficient to abrogate virtually all binding (Fig. S2A,B). Disruption of Ca^{2+} binding to the CaM C-lobe in the CaM₃₄ protein, which is defunct in its Ca^{2+} binding to the C-lobe but has native Ca^{2+} -binding capability for its N-lobe, also resulted in no significant interaction with the TRPV6 C-tail by analytical gel filtration (Fig. S2C) but CaM N-lobe specific shifts were observed in the ¹⁵N-¹H-HSQC spectrum (Fig. S2D), suggestive of a weak binder. In contrast, Ca^{2+} bound CaM₁₂, which has Ca^{2+} bound only to the CaM C-lobe was sufficient to facilitate strong TRPV6⁶⁵⁵⁻⁷²² binding, as evident from gel filtration (Fig. 1A), NMR

spectroscopy (Fig. 1B) and ITC (Fig. 1C). The CaM₁₂-TRPV6 complex displayed a ~1:1 stoichiometry with a K_d of 34 ± 3 nM indicative of a tight binding event. Weighted average chemical shift perturbations (CSPs, Fig 1D), which yield residue-specific information regarding the binding event, are observed exclusively for residues in the Ca²⁺-loaded C-lobe. Notably, the largest CSPs were observed for residues F92 and M144, which together make up a substantial part of the well-

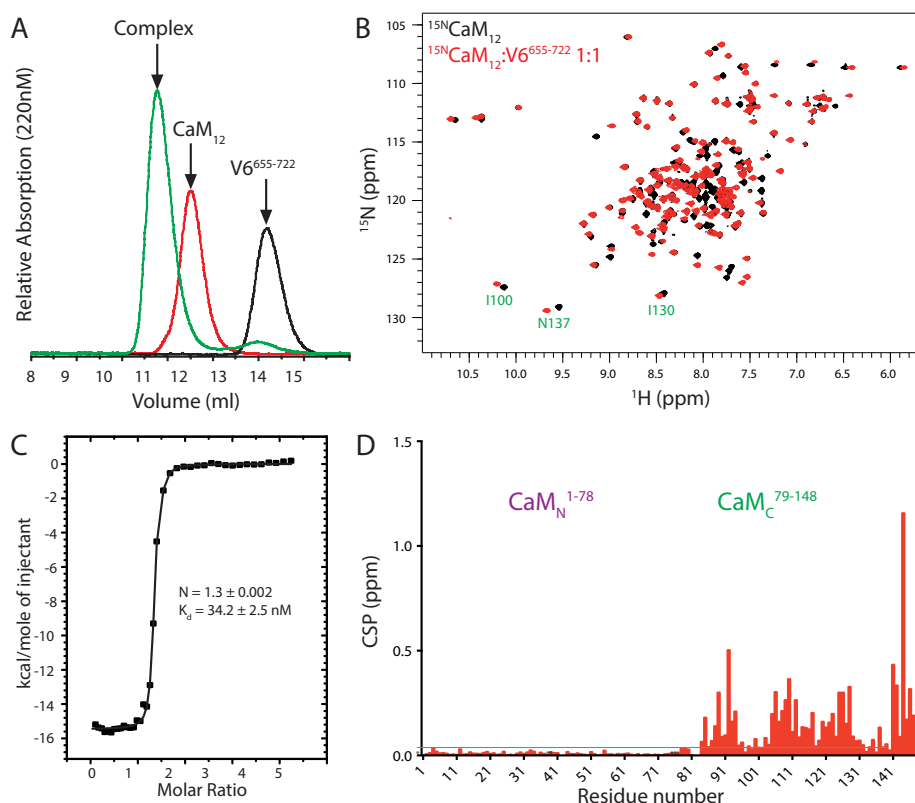


Figure 1- Analysis of TRPV6 C-tail binding to the Calmodulin N-lobe (CaM₁₂).

A) Analytical gel filtration curves are displayed for; free TRPV6⁶⁵⁵⁻⁷²² in black, free CaM₁₂ in red and the corresponding CaM₁₂:TRPV6⁶⁵⁵⁻⁷²² complex at a 1:1 molar ratio in green.

B) Overlay of the ¹⁵N-¹H-HSQC spectra of ¹⁵N-labelled CaM₁₂ (black) with the ¹⁵N-labelled CaM₁₂:TRPV6⁶⁵⁵⁻⁷²² complex (red) at a 1:1 molar ratio. Note that non-overlapping peaks identify residues affected by complex formation.

C) Representative ITC plot of CaM₁₂ titrated by TRPV6⁶⁵⁵⁻⁷²² and fitted using the one binding site model. Values for the number of binding sites N , together with the binding constant K_d are shown. Number of replicates equals 3.

D) CaM₁₂ chemical shift perturbation (CSP) ($\delta_{\text{bound}} - \delta_{\text{free}}$) as a function of residue number for the ¹⁵N-labelled CaM₁₂-TRPV6⁶⁵⁵⁻⁷²² complex at a molar ratio of 1:1. CSP values (ppm) were calculated as described in the materials and methods. A horizontal light blue line indicates the estimated absolute error.

characterised hydrophobic pocket of the CaM C-lobe that is formed upon binding Ca^{2+} ³⁷ and fully consistent with the structure of the $\text{CaM}_{12}:\text{TRPV5}^{655-725}$ complex⁵². We also tested the effect of the individual Ca^{2+} -binding sites in the CaM C-lobe using the CaM_{123} and CaM_{124} mutants to conclude that Ca^{2+} binding to site 4 in CaM is essential for the interaction with TRPV6 (Fig. S3). For the paralogue TRPV5 we also clearly established that a specific CaM:TRPV5 complex is formed under cellular basal Ca^{2+} conditions that involves a fully Ca^{2+} -loaded CaM C-lobe⁵² and hence, by analogy we infer the same molecular state for the CaM:TRPV6 complex.

Thus, based on these combined data we propose that, induced by the differential affinities of the CaM C- and N-lobes for Ca^{2+} , CaM first binds to the TRPV6 C-tail via critical contacts made solely within a fully Ca^{2+} -loaded C-lobe.

Elevated Ca^{2+} switches TRPV6 to a high Ca^{2+} -open state mediated via CaM N-lobe specific interactions

To further investigate the role of the CaM N-lobe in Ca^{2+} -mediated TRPV6 channel inactivation, we next assessed the interaction between $\text{TRPV6}^{655-722}$ and CaM under high- Ca^{2+} (10mM) conditions. Analysis of this interaction by ITC (Fig. 2A) revealed an initial tight binding event with a K_d 43 ± 11 nM, similar to that previously seen for CaM_{12} (cf. Fig. 1C). However, unlike the interaction of TRPV6 with CaM_{12} , in the presence of a Ca^{2+} -loaded CaM N-lobe, a second weaker interaction (9 μM) is also evident suggesting a two-step binding pattern (*vide infra*). NMR spectroscopy (Figs 2B,C) revealed that both CaM N- and CaM C-lobes now engage the TRPV6 C-tail, in marked contrast to the low- Ca^{2+} state exemplified by the CaM_{12} -TRPV6 complex. To determine which CaM residues are involved in the transition from the resting-open state ($\text{CaM}_{12}:\text{TRPV6}^{655-722}$) to the high- Ca^{2+} open-state ($\text{CaM}_{\text{WT}}:\text{TRPV6}^{655-722}$), we subtracted the CSPs for $\text{CaM}_{12}:\text{TRPV6}^{655-722}$ (Fig. 1D) from those obtained for $\text{CaM}_{\text{WT}}:\text{TRPV6}^{655-722}$ (Fig. 2C), effectively yielding the differential effects between the two complexes. The results of this analysis (Fig. 2D) clearly show that the major effects occur for CaM N-lobe residues with only minor changes observed for residues in the CaM C-lobe. In addition, the largest changes for the C-lobe occur for residues close in sequence to the N-lobe and are therefore likely due to their physical proximity to the N-lobe, rather than to a change in actual binding.

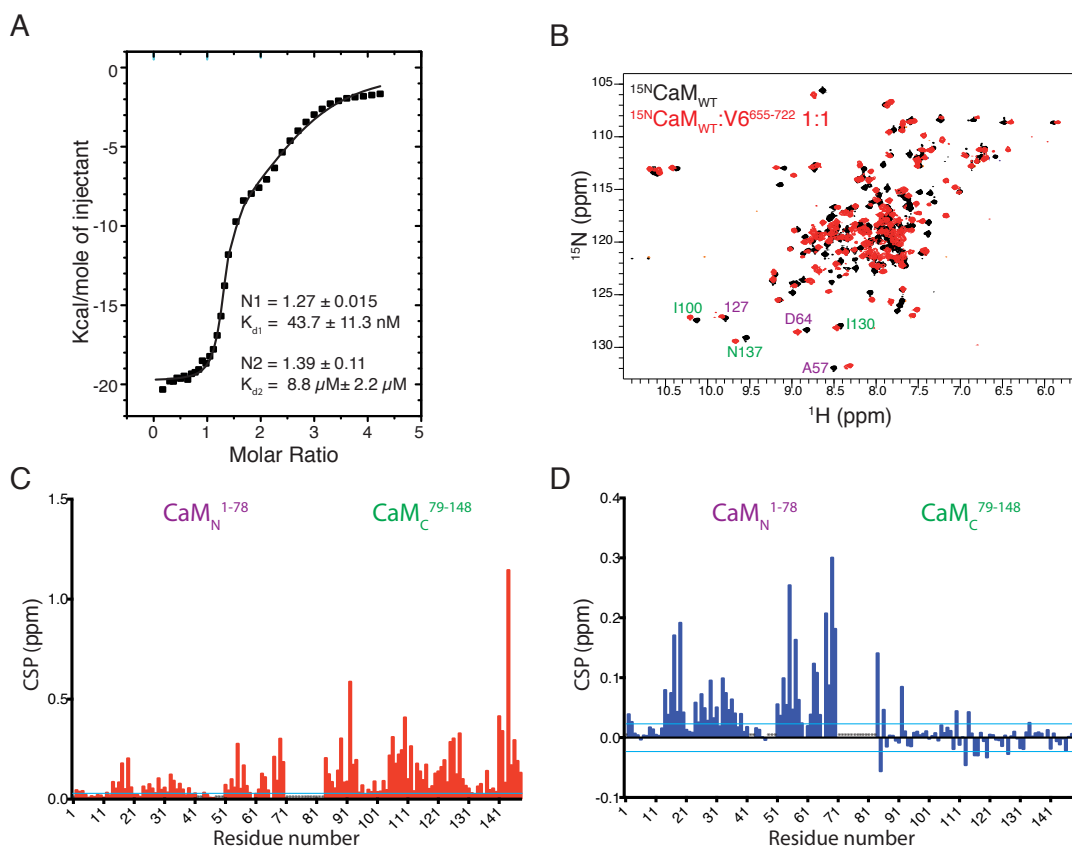


Figure 2- Analysis of TRPV6 C-tail binding to the fully Ca^{2+} -loaded Calmodulin (CaM_{WT}).

A) Representative ITC plot of CaM_{WT} titrated by $\text{TRPV6}^{655-722}$ and fitted using a two sites model. Values for the number of binding sites N , together with the binding constant K_d are shown. Number of replicates equals 3.

B) Overlay of the ^{15}N - ^1H -HSQC spectra of ^{15}N -labelled CaM_{WT} (black) and the ^{15}N -labelled $\text{CaM}_{\text{WT}}:\text{TRPV6}^{655-722}$ complex (red) at a 1:1 molar ratio.

C) CaM_{WT} chemical shift perturbations (CSPs) ($\delta_{\text{bound}} - \delta_{\text{free}}$) as a function of residue number for the ^{15}N -labelled $\text{CaM}_{\text{WT}}:\text{TRPV6}^{655-722}$ complex at a molar ratio of 1:1. CSP values (ppm) were calculated as described in the materials and methods.

D) CSP differences of the 1:1 $\text{CaM}_{\text{WT}}:\text{TRPV6}^{655-722}$ complex (as in C) and the 1:1 $\text{CaM}_{\text{I2}}:\text{TRPV6}^{655-722}$ complex (cf. Fig. 2D) as a function of residue number. Horizontal light blue lines in C) and D) indicate the estimated absolute error.

To date, the $\text{CaM}:\text{TRPV1}^{767-801}$ represents the only $\text{CaM}:\text{TRP}$ C-tail complex for which an atomic structure has been solved (PDB id 3SUI; Fig. 3A)³⁸. Under high Ca^{2+} conditions, $\text{CaM}:\text{TRPV1}^{767-801}$ adopts the typical closed canonical fold observed in many $\text{CaM}:\text{peptide}$ complexes³². Further analysis of the structure of this complex

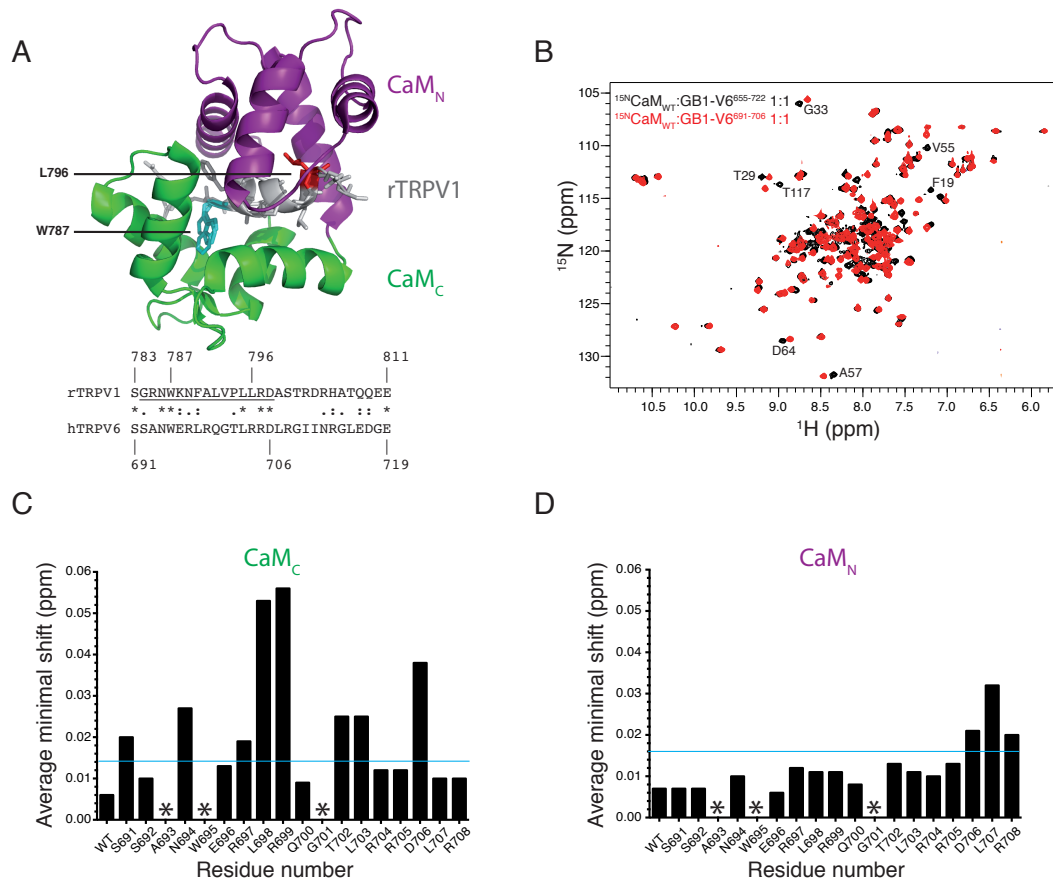


Figure 3- Analysis of the TRV6 C-tail CaM binding site.

A) Ribbon diagram of the crystal structure of the CaM:rTRPV1⁷⁶⁷⁻⁸⁰¹ C-tail complex (PDB: 3SUI)³⁶. The CaM N-lobe (purple), C-lobe (green) and the rTRPV1 peptide (grey) are indicated. Key rTRPV1 CaM N- and C-lobe residues are highlighted. Below: pairwise alignment between the rTRPV C-tail CaM binding region and the analogous region of TRPV6. The rTRPV1 region present in the crystal structure in (A) is underlined.

B) Overlay of the ¹⁵N-¹H-HSQC spectra of the 1:1 ¹⁵N-labelled CaM_{WT}:GB1-TRPV6⁶⁵⁵⁻⁷²² complex (black) with the 1:1 ¹⁵N-labelled CaM_{WT}:GB1-TRPV6⁶⁹¹⁻⁷⁰⁶ complex (red).

C) Alanine scanning mutagenesis of the TRPV6⁶⁵⁵⁻⁷²² C-tail CaM binding site. ¹⁵N-labelled CaM:mutant TRPV6⁶⁵⁵⁻⁷²² 1:1 complexes were analysed by ¹⁵N-¹H-HSQC NMR. Each bar represents the average of the minimal shift CSPs for the CaM_C lobe region, calculated as described in the materials and methods. Untested residues are labelled with an asterisk. A horizontal light blue bar indicates the estimated absolute error for the ¹⁵N-labelled CaM:TRPV6⁶⁵⁵⁻⁷²² 1:1 complex.

D) As for C) but calculated for the CaM_N lobe.

shows that the minimal TRPV1 CaM-interacting region comprises residues 784-798. In order to compare this CaM interacting region to the analogous 691-706 region within the TRPV6 fragment, we assembled the 1:1 ¹⁵N-CaM_{WT}:TRPV6^{GB1-655-722} and 1:1 ¹⁵N-CaM_{WT}:TRPV6^{GB1-691-706} complexes. Comparison of their ¹⁵N-¹H-HSQC

spectra (Fig. 3B) clearly indicates that residues outside of TRPV6 691-706 are also involved in this interaction. Furthermore, a qualitative analysis suggested that the differential effects predominantly involve residues specific to the CaM N-lobe, which can only be rationalised by a complex that is structurally distinct from the CaM:TRPV1 complex.

To assess the contributions of individual TRPV6 residues to lobe-specific CaM binding in the context of the longer C-tail fragment (655-722), we employed alanine-scanning mutagenesis. We excluded W695 as this residue has previously been shown to fully abrogate CaM binding¹⁸. The ability of each TRPV6 mutant protein to bind to ¹⁵N-CaM_{WT} under high Ca²⁺ conditions was assessed by ¹⁵N-¹H-HSQC and the data analysed using a minimal shift or nearest neighbour approach; this methodology has been shown to accurately reflect protein-protein interactions^{35,39}. Minimal shift analyses of fifteen ¹⁵N-CaM_{WT}:TRPV6 mutant protein complexes are shown in Fig. S4 with the mean shifts for the CaM C- and N-lobes presented in Figs 3C and 3D, respectively. Three distinct parts to the TRPV6 CaM binding region can be identified: a CaM C-lobe specific region comprised of residues S691-L703, a CaM N-lobe specific region encompassing residues L707-R708 and a hinge region formed by D706. Furthermore, this CaM:TRPV6 binding pattern suggests that, unlike TRPV1, under high-Ca²⁺ conditions TRPV6 induces a different CaM complex in which interactions occur independently across both CaM lobes.

In summary, the data show that in response to increasing [Ca²⁺] the CaM N-lobe becomes fully loaded with Ca²⁺, in which the CaM:TRPV6 complex is characterised by CaM N-lobe specific interactions with the C-terminal portion of the TRPV6 CaM binding site.

TRPV6 is inactivated by CaM_{WT} via a novel two-tail mechanism

The ITC data probing the interaction between TRPV6⁶⁵⁵⁻⁷²² and CaM_{WT} (Fig. 2A) showed the presence of a second weaker binding event, such that one CaM_{WT} can bind two TRPV6⁶⁵⁵⁻⁷²² moieties. NMR spectroscopy of the CaM_{WT} and TRPV6⁶⁵⁵⁻⁷²² complexes at 1:1 and 1:2 molar ratios (Figs 4A,B) showed that significant changes arising from the binding of the second TRPV6 moiety are almost exclusively observed for the CaM N-lobe. Interestingly, the most affected residues are part of the hydrophobic pocket on the N-lobe (Fig. 4C), which is formed when it binds Ca²⁺³⁷.

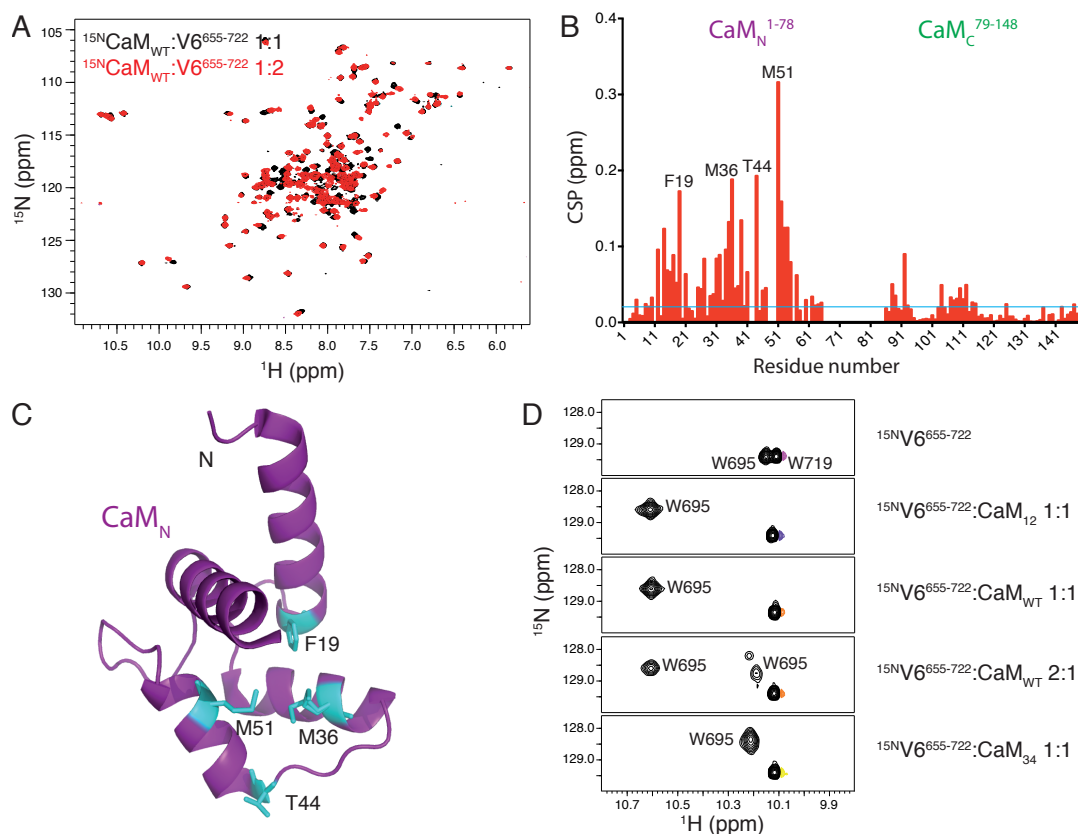


Figure 4- Analysis of the second TRPV6 C-tail CaM binding site.

A) Overlay of the ^{15}N - ^1H -HSQC CaM spectra of the 1:1 ^{15}N -labelled $\text{CaM}_{\text{WT}}:\text{TRPV6}^{655-722}$ complex (black) with the 1:2 ^{15}N -labelled $\text{CaM}_{\text{WT}}:\text{TRPV6}^{655-722}$ complex (red).

B) CaM_{WT} chemical shift perturbation (CSP) ($\delta_{\text{bound 1:2}} - \delta_{\text{bound 1:1}}$) as a function of residue number for the 1:2 ^{15}N -labelled $\text{CaM}_{\text{WT}}:\text{TRPV6}^{655-722}$ complex compared to the 1:1 complex. CSP values (ppm) were calculated as described in the materials and methods. The horizontal light blue line indicates the estimated absolute error. The four residues with the largest CSPs are highlighted.

C) Ribbon diagram of the CaM N-lobe (purple) of the $\text{CaM}:\text{rTRPV1}^{767-801}$ C-tail complex (PDB: 3SUI)³⁶. Highlighted residues from B) are shown as sticks (cyan).

D) Zoomed regions of various ^{15}N - ^1H -HSQC spectra of ^{15}N -labelled $\text{TRPV6}^{655-722}$ in complex with different Ca^{2+} bound forms of CaM. The indole ring amino group of the tryptophan side chains for residues W695 and W719 are marked.

We then assessed the role of W695 in formation of the 1:2 complex. Two tryptophan residues are present in the $\text{TRPV6}^{655-722}$ construct; W695 and W719, whose side-chain indole amino groups present convenient probes to monitor the interaction by recording ^{15}N - ^1H -HSQC spectra of ^{15}N - $\text{TRPV6}^{655-722}$ and its various CaM complexes (Fig. 4D). As expected neither CaM_{WT} , nor the various mutant CaMs, affect the W719 cross-peak, consistent with the notion that this residue does not participate in binding. However, the cross-peak of W695 is strongly shifted upon

addition of CaM₁₂, binding to the CaM C-lobe in line with its proposed crucial role in complex formation¹⁸ and the CaM₁₂:TRPV5 structure⁵². Conversely, a unique cross peak position is observed for the 1:1 CaM₃₄:¹⁵N-TRPV6⁶⁵⁵⁻⁷²² complex, in which only the CaM N-lobe is Ca²⁺-bound and engages with the TRPV6⁶⁵⁵⁻⁷²² moiety. Comparison of the 1:1 CaM₁₂:¹⁵N-TRPV6⁶⁵⁵⁻⁷²² complex with the 1:1 CaM_{WT}:¹⁵N-TRPV6⁶⁵⁵⁻⁷²² complex shows an identical pattern for both complexes, indicating that W695 is bound to the CaM C-lobe in both instances. Interestingly, upon formation of the 1:2 CaM_{WT}:¹⁵N-TRPV6⁶⁵⁵⁻⁷²² complex, a W695 cross-peak appears at a spectral location similar to the cross-peak observed for the 1:1 CaM₃₄:¹⁵N-TRPV6⁶⁵⁵⁻⁷²² complex. Thus, we conclude that in the 1:2 CaM_{WT}:¹⁵N-TRPV6⁶⁵⁵⁻⁷²² complex one TRPV6 tail is bound to the CaM C-lobe via its W695 residue, while a second TRPV6 C-tail is bound to the CaM N-lobe via its W695 residue.

To further investigate the role of the critical TRPV6-CaM N-lobe interactions on channel inactivation we decided to focus on the L707 residue, which we identified as a CaM N-lobe specific interactor from the alanine scanning mutagenesis (Figs 3C-D). Therefore, we evaluated the binding of the TRPV6⁶⁵⁵⁻⁷²² L707A mutant to CaM_{WT} by NMR spectroscopy (Figs 5A, B) and ITC (Fig. 5C). CSP analysis shows changes predominantly for residues in the CaM_{WT} N-lobe, with minor changes seen for the C-lobe residues closest to the N-lobe. The latter probably arise indirectly from a proximity effect. Interestingly, the most-affected residues cluster in the hydrophobic pocket (Fig. 5B) also identified for the 2;1 interaction. The mutation has increased the affinity of TRPV6⁶⁵⁵⁻⁷²² L707A for CaM_{WT} for the first binding event by ~2-fold, but significantly, increased the affinity of the second binding event by 10-fold.

If the formation of the 1:2 complex has a functional role, the increased affinity of the second binding event resulting from the L707A mutation would be expected to stabilise the inactivated state and thus increase the rate of channel inactivation. Hence, the effect of the L707A mutation in the context of the intact channel was investigated by measuring channel inactivation in mammalian cells. TRPV6 mediated currents were recorded by whole-cell voltage clamp in HEK293 cells expressing either WT or mutant L707A channels. We ensured proper control of intra-cellular Ca²⁺ during cell culturing and experiment preparation (see methods) and leak currents were measured prior to the extracellular solution being exchanged for high Ca²⁺ conditions.

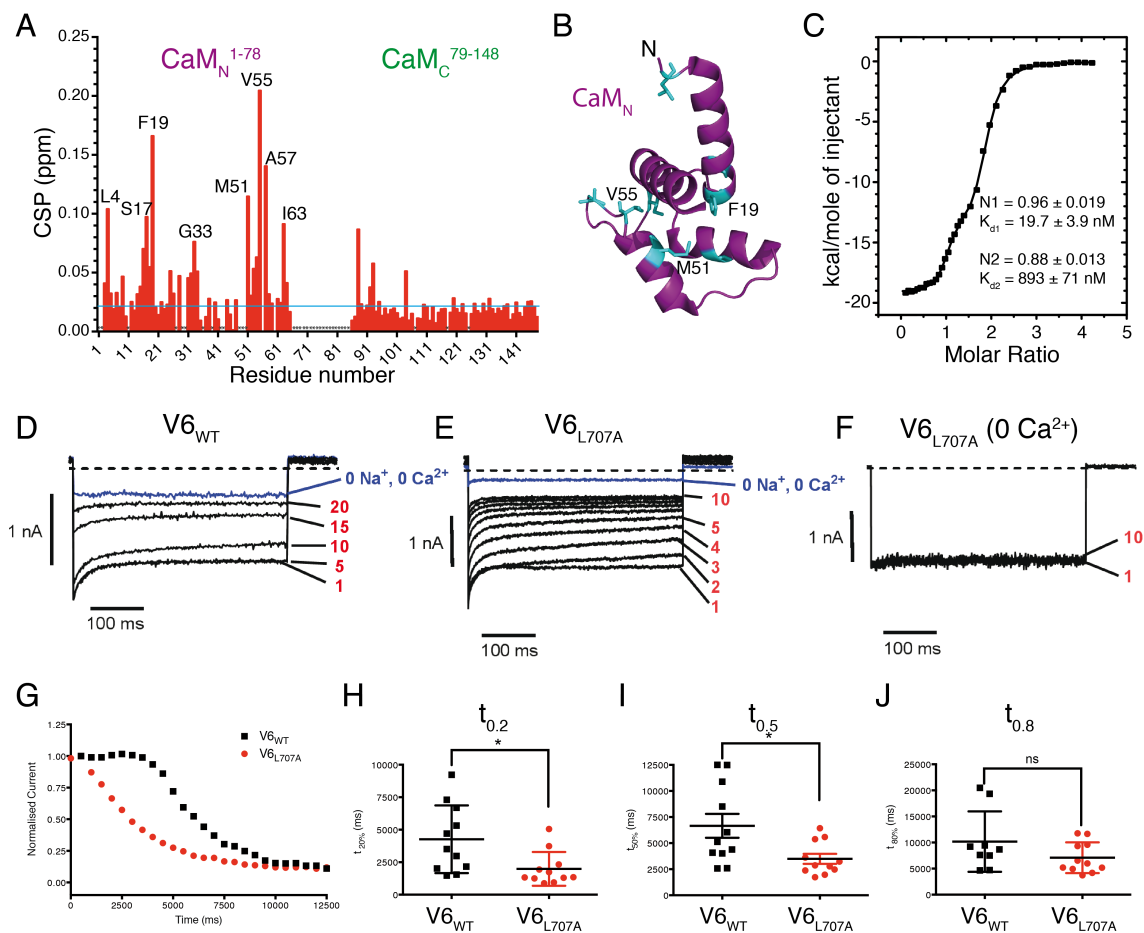


Figure 5- Characterisation of the TRPV6⁶⁵⁵⁻⁷²² L707A mutant.

A) CaM_{WT} chemical shift perturbation (CSP) ($\delta_{\text{boundV6L707A}} - \delta_{\text{boundV6WT 1:1}}$) as a function of residue number for the 1:1 ¹⁵N-labelled CaM_{WT}-TRPV6^{655-722(L707A)} mutant complex. CSP values (ppm) were calculated as described in the materials and methods. A horizontal light blue line indicates the estimated absolute error. Residues with the largest CSP are highlighted.

B) Ribbon diagram of the CaM N-lobe (purple) of the CaM:rTRPV1⁷⁶⁷⁻⁸⁰¹ C-tail complex (PDB: 3SUI). Highlighted residues from A) are shown as sticks (cyan).

C) Representative ITC plot of CaM_{WT} titrated by the TRPV6^{655-722(L707A)} mutant and fitted using the two sites model. Values for the number of binding sites N, together with the binding constant K_d are shown. Number of replicates equals 2.

D-E) Representative WT (D) and L707A (E) TRPV6 whole cell current traces elicited by repetitively pulsing to 100 mV. Currents were first recorded in an NMDG-based (0 Na⁺, 0 Ca²⁺) solution, then switched to a normal Na⁺ + Ca²⁺ based solution. For clarity, only selected traces, different for each panel, are shown with the corresponding pulse number indicated to the right of each panel. Note that WT currents are superimposed for the first 5 pulses, whereas L707A currents decrease substantially during the same time-frame.

F) Representative L707A TRPV6 whole cell current recordings from a cell perfused with 0 Ca²⁺ (0 mM Ca²⁺, 2 mM EGTA) NaCl-based extracellular solution. Currents showed no fast or slow components of inactivation in the absence of extracellular Ca²⁺ (for clarity, only first 10 current traces are shown).

(G) Representative time courses of Ca²⁺-dependent current inactivation for WT and L707A TRPV6 currents. Peak currents with each voltage pulse were normalised to peak current at pulse 1 and plotted against time. Each symbol represents normalised current from a single voltage pulse.

(H-J) Time to 20, 50 and 80 % inactivation. Each symbol is a measure from a single cell. Horizontal lines indicate mean \pm SEM. * $p < 0.05$. ns – not significant.

Representative TRPV6 and TRPV6 L707A currents recorded in control solutions in response to 500 ms repetitive pulsing to -100 mV at a frequency of 1 Hz are shown in Figs 5D-E. As reported previously^{18,40}, two components of inactivation were observed, a rapid onset component (complete in \sim 50 ms) and a slow component. Whereas the fast component rapidly recovered between pulses, after an initial delay the slow component resulted in a progressive reduction of current amplitude with repetitive pulsing (Fig. 5G). Currents could also be observed to slowly and fully recover from inactivation over a period of several minutes under conditions of reduced Ca²⁺ entry (50 ms duration pulses applied at 10 s intervals; data not shown) and inactivation was abolished in solutions without extracellular Ca²⁺ (Fig. 5F), indicating that both components of inactivation were Ca²⁺ dependent and current run-down was minimal. Mean maximum inactivation for TRPV6 and TRPV6-L707 was $86 \pm 3 \%$ (n=10) and $90 \pm 1.6 \%$ (n=12), respectively. Figs 5G-I show that inactivation of TRPV6 L707A currents was significantly faster when compared to TRPV6. The mean times to 20% ($t_{0.2}$) and 50% ($t_{0.5}$) inactivation were 4300 ± 790 ms and 6600 ± 1100 ms, respectively, for TRPV6. These were significantly reduced to 1990 ± 390 ms and 3500 ± 480 ms, respectively, for TRPV6 L707A (Figs 5H, I). Mean current amplitudes of TRPV6 L707A were -1600 ± 200 pA (n=11), which was significantly higher than -1050 ± 100 pA (n=11) for TRPV6. We considered the possibility that the faster inactivation of TRPV6 L707A was due to larger currents and greater Ca²⁺ influx. However, the correlation between current amplitude and $t_{0.5}$ inactivation for the combined TRPV6 and TRPV6 L707A data was poor (Pearson R² value 0.46, n = 22) and even lower for the TRPV6 L707A data alone (Pearson R² value 0.23, n = 11). Thus, we conclude that the TRPV6 L707A mutation increases the rate of inactivation of functional channels in a manner consistent with the effects of this mutation on CaM binding affinity.

Discussion

The epithelial TRPV5 and TRPV6 Ca^{2+} -channels play an important role in Ca^{2+} homeostasis, and their functioning is tightly controlled by a Ca^{2+} -dependent feedback mechanism(s) to facilitate channel inactivation. Calcium CaM-dependent TRPV6 channel inactivation involves the very C-terminal part of the channel, which is unfortunately either absent or unresolved in the atomic resolution structures of TRPV6^{8,9}. Here, we have used a range of biophysical techniques to characterise the interactions of CaM with the TRPV6 C-terminal tail that underpin the mechanism of channel inactivation. We deduce that this mechanism involves three distinct states of the CaM:TRPV6 complex and propose a so-called “two-tail” model to rationalise our findings (cf. Fig. 6): The model comprises: 1) a “resting Ca^{2+} -open state” formed under basal cellular $[\text{Ca}^{2+}]$ of ~ 100 nM where calmodulin (CaM) engages the C-tail via CaM C-lobe interactions and the CaM N-lobe is in an apo state; 2) a “high- Ca^{2+} open-state” is formed when an increased cellular $[\text{Ca}^{2+}]$ loads the apo CaM N-lobe with Ca^{2+} and the C-tail can now engage the CaM N-lobe via a crucial TRPV6^{L707}:CaM N-lobe specific interaction; 3) a “high- Ca^{2+} inactivated state” is formed when the channel engages CaM via a novel mechanism, whereby a second C-tail displaces the first C-tail from the CaM N-lobe to form a complex which bridges

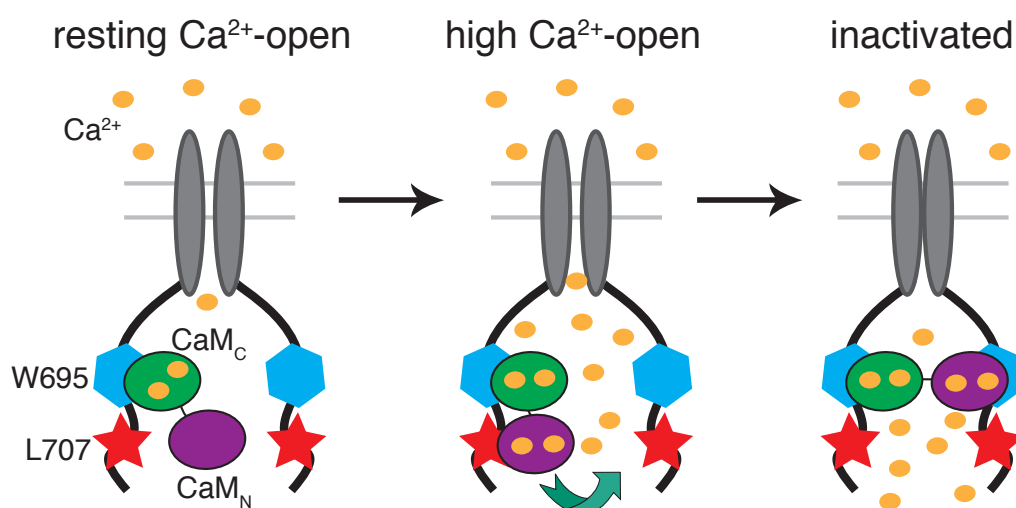


Figure 6- Schematic of the “two-tail” model of CaM-mediated TRPV regulation. Note only two of the four TRPV channel subunits are represented. Differential C- or N-lobe dependent interactions (indicated) characterise the resting Ca^{2+} -open, high Ca^{2+} -open and inactivated states. Leucine 707 is crucial in the switch to the 1:2 CaM:TRPV6 complex that results in an inactivated channel.

between two monomers and is coupled to closure of the channel pore.

Our data show that the low Ca^{2+} -mimicking CaM_{12} -mutant forms a tight complex mediated by only the CaM C-lobe (Fig. 1) and under resting intracellular Ca^{2+} levels (~ 100 nM) the C-tail of the TRPV6 paralogue, TRPV5, is constitutively bound to CaM^{52} . Moreover, under these conditions the CaM C-lobe is fully Ca^{2+} loaded whilst the N-lobe remains Ca^{2+} free. This is in line with previous observations, which showed that in HEK293 cells at an intracellular $[\text{Ca}^{2+}]$ of 200 nM none of the ~ 10 μM total cellular CaM is fully Ca^{2+} -loaded⁴¹. In addition, a TRPV1-CaM complex was successfully purified from HEK293 cells using immunoprecipitation experiments²⁸, also indicating a tight association between the channel and CaM under native conditions. Furthermore, live-cell FRET experiments of voltage-gated Ca^{2+} ion channels showed constitutive association of CaM with the channel under a low intracellular $[\text{Ca}^{2+}]$ ⁴². However in contrast, live-cell FRET experiments of TRPV6 suggested a $[\text{Ca}^{2+}]$ -dependent association of the channel with CaM, rather than a constitutive one¹⁷. In these latter experiments, the fluorophore was tagged on to the N-terminus of the CaM N-lobe and therefore was most likely monitoring the induced association of the CaM N-lobe with the channel, as postulated by our high- Ca^{2+} open-state 1:1 CaM:TRPV6 complex, rather than a direct CaM C-lobe mediated channel interaction.

In direct response to elevated $[\text{Ca}^{2+}]$ CaM is further Ca^{2+} -loaded at its N-lobe, thus extending the high affinity binding surface to include both the C- and N-lobes. This establishes the high- Ca^{2+} open-state 1:1 CaM:TRPV6 complex (Figs 2C,D). In order to identify the key TRPV6 residues essential for the formation of this complex, we employed alanine scanning mutagenesis and assessed the ability of each TRPV6 mutant to bind to CaM_{WT} . This analysis identified three distinct parts to the TRPV6 CaM binding interface, with the region S691-L703 functioning as the primary region for the CaM C-lobe interaction (Fig. 3C) and by analogy the residues involved in the CaM_{12} interaction. This region is highly conserved between TRPV6⁶⁹¹⁻⁷⁰³ (SSANWERLRQGTL) and the equivalent part from TRPV5⁶⁹⁸⁻⁷¹⁰ (SHRGWEILRQNTL), with the latter extensively tested using electrophysiology experiments. Mutagenesis of the TRPV5 residues only increased Ca^{2+} uptake in HEK293 cells, most likely due to a reduced ability to bind CaM^{23} . Significantly, none of the mutations tested resulted in a reduced Ca^{2+} uptake i.e. suggestive of channel

inactivation. Furthermore, the critical CaM N-lobe interacting TRPV6 region (⁷⁰⁴RRDLR⁷⁰⁸) identified in this study is not conserved within TRPV5 (⁷¹⁰GHLNL⁷¹⁴). The full-length TRPV6 L707A mutant channel showed a significantly faster inactivation in our electrophysiology experiments (Figs 5D-J), which cannot be rationalised by a loss of the CaM:TRPV6 interaction. Finally, this effect constitutes the first observation of a mutation in a TRPV channel that results in faster inactivation; thus far all other mutations were only shown to abrogate the inactivation process.

In the X-ray structure of CaM and the related TRPV1 C-tail³⁸ TRPV1 residues 784-798 are tightly embedded in a classical antiparallel ‘closed’ CaM conformation, simultaneously contacting both N- and C-lobes in a so-called 1-10 interaction motif (Fig. 3A). Our data indicate that the 1:1 CaM:TRPV6 complex is different, with separate regions of TRPV6 contacting either the N-lobe or the C-lobe exclusively (Figs 3C,D). Given the high degree of similarities of the C-lobe CSP patterns of the CaM₁₂ and CaM_{WT} complexes for both TRPV6 (Figs 1D and 2C) and TRPV5⁵², the conformation of the C-lobe in complex with the channel tail is expected to be very similar in all cases. The complex of CaM₁₂ with the TRPV6 paralogue TRPV5 displays a 1-5-8 CaM interaction motif, with a fully disengaged N-lobe⁵² allowing for full adaptability of its orientation. We searched the PDB repository for structures of CaM_{WT}:target complexes that could present a more suitable model for the fully Ca²⁺-loaded 1:1 CaM_{WT}:TRPV6 complex. Three 1:1 CaM_{WT}:peptide complexes, i.e. Munc13-1:CaM⁴³, α II-spectrin:CaM⁴⁴ and Matrix domain of HIV-1 gag:CaM⁴⁵, were identified that each have a conserved tryptophan residue bound to the CaM C-lobe, similarly to TRPV6 and TRPV5, with a second hydrophobic residue bound to the CaM N-lobe, again similar to TRPV6. The peptides bind antiparallel to the CaM N- and C-lobes and the CaM N- and C-lobes display a much more open conformation. Interestingly, the larger the number of residues between the C-lobe bound tryptophan and the N-lobe bound hydrophobic residue, the more open the complex becomes. By sequence analogy alone, the CaM_{WT}:TRPV6 complex would be expected to resemble the α II-spectrin:CaM complex (PDB code 2FOT), while simultaneously suggesting that the peptide used in the X-ray studies of the CaM:TRPV1 complex may have been too short at the C-terminus to fully capture the analogous effects as reported in this study for TRPV6.

Until now, the full molecular mechanism(s) of TRP channel inactivation by CaM have been elusive. The most popular hypothesis, formulated for the TRPV1 and TRPV4 channels, proposes the formation of a ternary complex such that CaM bridges the channels N- and C-termini via N-tail-CaM N-lobe and CaM C-lobe C-tail complexes. Potentially, the formation of such a ternary complex could involve the distinct CaM N-lobe mediated second interaction surface we observed in the 1:2 CaM:TRPV6 complex. However, within the TRPV subfamily CaM_{WT} has only been shown to bind to the N-terminal cytosolic domain of TRPV1, TRPV3 and TRPV4 and not to TRPV2, TRPV5 or TRPV6⁴⁶, rendering this mode of interaction for channel inactivation of the latter and potentially the whole TRPV sub-family, unlikely. Moreover, attempts to form such a complex for TRPV1 have so far proven unsuccessful³⁸. In contrast, our two-tail hypothesis is backed by experimental data that include the formation of a specific 1:2 CaM:TRPV6 complex (Fig. 4) and fully explains the effects of the L707A mutation (Fig. 5) whereas the N-tail/C-tail CaM bridging model fails to explain the resulting experimentally observed effects.

Our two-tail model hinges on the charging of the CaM N-lobe as the crucial Ca²⁺-sensing step with the C-tails not fully charged with CaM under basal Ca²⁺ conditions, i.e. dependent on the local availability of the partially Ca²⁺ loaded CaM. Once fully charged with Ca²⁺, the C-terminal region of the TRPV6 C-tail CaM binding site engages with the newly created hydrophobic pocket on the N-lobe via its L707 residue. Concomitantly, our model postulates that W695 from a second TRPV6 C-tail competes and displaces L707 from the hydrophobic pocket, thus using CaM to form a bridge between two TRPV6 C-tails resulting in channel inactivation (Fig. 6). This mode of binding has also been observed in the structures of CaM with petunia glutamate decarboxylase, where two C-tail peptides interact simultaneously; each via a single tryptophan residue with either the CaM N- or C-lobes to form a 1:2 CaM:peptide complex^{47,48}. In addition, a similar structure was also determined for CaM interacting with the CaM binding domain of the tetrameric Orai1 channel, where a 1:2 CaM:channel complex was shown to occur *in vitro*⁴⁹. Finally a pseudo-atomic structure of full-length tetrameric aquaporin-0 in complex with CaM⁵⁰ infers a mechanism of CaM mediated channel inactivation similar to the one proposed here for TRPV6.

In conclusion, our data underpins a novel “two-tail” model for the CaM-mediated inactivation of the TRPV6 channel. This model comprises three dynamically connected states in which differential interactions between the C-tails within the tetrameric channel and the CaM N- and C-lobes form the defining elements. Using a structure and interaction driven approach, we have characterised the crucial molecular components for each stage. Notably, we have identified the CaM N-lobe-mediated 1:2 CaM:TRPV6 complex formation as the key event that leads to channel inactivation. We have shown that the L707A mutation resulted in a significant increase in the rate of channel inactivation; an effect never previously observed within the TRPV family and that can only be explained by our “two-tail” model of CaM mediated TRPV channel inactivation.

Acknowledgements

We thank Dr. Fred Muskett for expert support and maintenance of our NMR equipment. GWV acknowledges funding during various stages of this project by BBSRC (grant BB/J007897/1) and MRC (grants MR/L000555/1 and MR/P00038X/1).

Supplementary materials

Four Figures: evaluation of the integrity of all the CaM mutants, assessment of CaM₁₂₃₄, CaM₁₂₃, CaM₁₂₄ and CaM₃₄ binding to the TRPV⁶⁵⁵⁻⁷²² fragment, and the full NMR analysis of all fifteen TRPV⁶⁵⁵⁻⁷²² mutants.

References

- (1) Montell, C. (2005) The TRP Superfamily of Cation Channels. *Science Signaling* 2005, re3–re3.
- (2) Nilius, B., and Owsianik, G. (2010) Transient receptor potential channelopathies. *Pflugers Arch.* 460, 437–450.
- (3) Chen, J., Luan, Y., Yu, R., Zhang, Z., Zhang, J., and Wang, W. (2014) Transient receptor potential (TRP) channels, promising potential diagnostic and therapeutic tools for cancer. *BST* 8, 1–10.
- (4) Liao, M., Cao, E., Julius, D., and Cheng, Y. (2013) Structure of the TRPV1 ion channel determined by electron cryo-microscopy. *Nature* 504, 107–112.
- (5) Zubcevic, L., Herzik, M. A., Chung, B. C., Liu, Z., Lander, G. C., and Lee, S.-Y. (2016) Cryo-electron microscopy structure of the TRPV2 ion channel. *Nat Struct Mol Biol* 23, 180–186.
- (6) Hughes, T. E. T., Lodowski, D. T., Huynh, K. W., Yazici, A., Del Rosario, J., Kapoor, A., Basak, S., Samanta, A., Han, X., Chakrapani, S., Zhou, Z. H., Filizola, M., Rohacs, T., Han, S., and Moiseenkova-Bell, V. Y. (2018) Structural basis of TRPV5 channel inhibition by econazole revealed by cryo-EM. *Nat Struct Mol Biol* 1–12.
- (7) Paulsen, C. E., Armache, J.-P., Gao, Y., Cheng, Y., and Julius, D. (2015) Structure of the TRPA1 ion channel suggests regulatory mechanisms. *Nature* 520, 511–517.
- (8) Saotome, K., Singh, A. K., Yelshanskaya, M. V., and Sobolevsky, A. I. (2016) Crystal structure of the epithelial calcium channel TRPV6. *Nature* 534, 506–511.
- (9) McGoldrick, L. L., Singh, A. K., Saotome, K., Yelshanskaya, M. V., Twomey, E. C., Grassucci, R. A., and Sobolevsky, A. I. (2018) Opening of the human epithelial calcium channel TRPV6. *Nature* 553, 233–237.
- (10) Li, M., Yu, Y., and Yang, J. (2010) Structural Biology of TRP Channels, in *Advances in Experimental Medicine and Biology*, pp 1–23. Springer Netherlands, Dordrecht.
- (11) Hoenderop, J. G. J. (2005) Calcium Absorption Across Epithelia. *Physiological Reviews* 85, 373–422.
- (12) Peng, J.-B., Chen, X.-Z., Berger, U. V., Weremowicz, S., Morton, C. C., Vassilev, P. M., Brown, E. M., and Hediger, M. A. (2000) Human Calcium

- Transport Protein CaT1. *Biochem. Biophys. Res. Commun.* 278, 326–332.
- (13) Vennekens, R., Hoenderop, J., Prenen, J., Stuiver, M., Willems, P., Droogmans, G., Nilius, B., and Bindels, R. (2000) Permeation and gating properties of the novel epithelial Ca²⁺ channel. *J. Biol. Chem.* 275, 3963–3969.
- (14) Hoenderop, J., van der Kemp, A., Hartog, A., van de Graaf, S., van Os, C. H., Willems, P., and Bindels, R. (1999) Molecular identification of the apical Ca²⁺ channel in 1,25-dihydroxyvitamin D-3-responsive epithelia. *J. Biol. Chem.* 274, 8375–8378.
- (15) Hoenderop, J. G. J., van Leeuwen, J. P. T. M., van der Eerden, B. C. J., Kersten, F. F. J., van der Kemp, A. W. C. M., Mérellat, A.-M., Waarsing, J. H., Rossier, B. C., Vallon, V., Hummler, E., and Bindels, R. J. M. (2003) Renal Ca²⁺ wasting, hyperabsorption, and reduced bone thickness in mice lacking TRPV5. *J. Clin. Invest.* 112, 1906–1914.
- (16) Weissgerber, P., Kriebs, U., Tsvilovskyy, V., Olausson, J., Kretz, O., Stoerger, C., Mannebach, S., Wissenbach, U., Vennekens, R., Middendorff, R., Flockerzi, V., and Freichel, M. (2012) Excision of Trpv6 Gene Leads to Severe Defects in Epididymal Ca²⁺ Absorption and Male Fertility Much Like Single D541A Pore Mutation. *Journal of Biological Chemistry* 287, 17930–17941.
- (17) Derler, I., Hofbauer, M., Kahr, H., Fritsch, R., Muik, M., Kepplinger, K., Hack, M. E., Moritz, S., Schindl, R., Groschner, K., and Romanin, C. (2006) Dynamic but not constitutive association of calmodulin with rat TRPV6 channels enables fine tuning of Ca²⁺-dependent inactivation. *The Journal of Physiology* 577, 31–44.
- (18) Cao, C., Zakharian, E., Borbiri, I., and Rohacs, T. (2013) Interplay between Calmodulin and Phosphatidylinositol 4,5-Bisphosphate in Ca²⁺-induced Inactivation of Transient Receptor Potential Vanilloid 6 Channels. *Journal of Biological Chemistry* 288, 5278–5290.
- (19) Lambers, T. T., Mahieu, F., Oancea, E., Hoofd, L., de Lange, F., Mensenkamp, A. R., Voets, T., Nilius, B., Clapham, D. E., Hoenderop, J. G., and Bindels, R. J. (2006) Calbindin-D-28K dynamically controls TRPV5-mediated Ca²⁺ transport. *Embo Journal* 25, 2978–2988.
- (20) Gkika, D., Mahieu, F., Nilius, B., Hoenderop, J. G. J., and Bindels, R. J. M. (2004) 80K-H as a New Ca²⁺ Sensor Regulating the Activity of the Epithelial

- Ca²⁺ Channel Transient Receptor Potential Cation Channel V5 (TRPV5). *Journal of Biological Chemistry* 279, 26351–26357.
- (21) Niemeyer, B. A., Bergs, C., Wissenbach, U., Flockerzi, V., and Trost, C. (2001) Competitive regulation of Ca²⁺-like-mediated Ca²⁺ entry by protein kinase C and calmodulin. *Proc. Natl. Acad. Sci. U.S.A.* 98, 3600–3605.
- (22) Lambers, T. T., Weidema, A. F., Nilius, B., Hoenderop, J. G. J., and Bindels, R. J. M. (2004) Regulation of the Mouse Epithelial Ca²⁺ Channel TRPV6 by the Ca²⁺-sensor Calmodulin. *Journal of Biological Chemistry* 279, 28855–28861.
- (23) de Groot, T., Kovalevskaya, N. V., Verkaart, S., Schilderink, N., Felici, M., van der Hagen, E. A. E., Bindels, R. J. M., Vuister, G. W., and Hoenderop, J. G. (2011) Molecular Mechanisms of Calmodulin Action on TRPV5 and Modulation by Parathyroid Hormone. *Molecular and Cellular Biology* 31, 2845–2853.
- (24) Kovalevskaya, N. V., Bokhovchuk, F. M., and Vuister, G. W. (2012) The TRPV5/6 calcium channels contain multiple calmodulin binding sites with differential binding properties. *J Struct Funct Genomics* 13, 91–100.
- (25) Kovalevskaya, N. V., Schilderink, N., and Vuister, G. W. (2011) Expression and purification of the C-terminal fragments of TRPV5/6 channels. *Protein Expression and Purification* 80, 28–33.
- (26) Nilius, B., Weidema, F., Prenen, J., Hoenderop, J. G., Vennekens, R., Hoefs, S., Droogmans, G., and Bindels, R. J. (2003) The carboxyl terminus of the epithelial Ca²⁺ channel ECaC1 is involved in Ca²⁺-dependent inactivation. *Pflugers Arch.* 445, 584–588.
- (27) Singh, B. B., Liu, X. B., Tang, J. S., Zhu, M. X., and Ambudkar, I. S. (2002) Calmodulin regulates Ca²⁺-dependent feedback inhibition of store-operated interaction with a site in the Ca²⁺ influx by C terminus of TrpC1. *Molecular Cell* 9, 739–750.
- (28) Numazaki, M., Tominaga, T., Takeuchi, K., Murayama, N., Toyooka, H., and Tominaga, M. (2003) Structural determinant of TRPV1 desensitization interacts with calmodulin. *Proc. Natl. Acad. Sci. U.S.A.* 100, 8002–8006.
- (29) Strotmann, R., Schultz, G., and Plant, T. D. (2003) Ca²⁺-dependent Potentiation of the Nonselective Cation Channel TRPV4 Is Mediated by a C-terminal Calmodulin Binding Site. *Journal of Biological Chemistry* 278, 26541–26549.
- (30) Mercado, J., Gordon-Shaag, A., Zagotta, W. N., and Gordon, S. E. (2010) Ca²⁺-

Dependent Desensitization of TRPV2 Channels Is Mediated by Hydrolysis of Phosphatidylinositol 4,5-Bisphosphate. *Journal of Neuroscience* 30, 13338–13347.

- (31) Kovalevskaya, N. V., van de Waterbeemd, M., Bokhovchuk, F. M., Bate, N., Bindels, R. J. M., Hoenderop, J. G. J., and Vuister, G. W. (2013) Structural analysis of calmodulin binding to ion channels demonstrates the role of its plasticity in regulation. *Pflugers Arch.* 465, 1507–1519.
- (32) Tidow, H., and Nissen, P. (2013) Structural diversity of calmodulin binding to its target sites. *FEBS J.* 280, 5551–5565.
- (33) Linse, S., Helmersson, A., And Forsen, S. (1991) Calcium-Binding to Calmodulin and Its Globular Domains. *J. Biol. Chem.* 266, 8050–8054.
- (34) Bate, N., Gingras, A. R., Bachir, A., Horwitz, R., Ye, F., Patel, B., Goult, B. T., and Critchley, D. R. (2012) Talin contains a C-terminal calpain2 cleavage site important in focal adhesion dynamics. *PLoS ONE* 7, e34461.
- (35) Williamson, R. A., Carr, M. D., Frenkiel, T. A., Feeney, J., and Freedman, R. B. (1997) Mapping the binding site for matrix metalloproteinase on the N-terminal domain of the tissue inhibitor of metalloproteinases-2 by NMR chemical shift perturbation. *Biochemistry* 36, 13882–13889.
- (36) Wu, P.-R., Kuo, C.-C., Yet, S.-F., Liou, J.-Y., Wu, K. K., and Chen, P.-F. (2012) Lobe-Specific Calcium Binding in Calmodulin Regulates Endothelial Nitric Oxide Synthase Activation. *PLoS ONE* (Hofmann, A., Ed.) 7, e39851.
- (37) Babu, Y. S., Bugg, C. E., and Cook, W. J. (1988) Structure of calmodulin refined at 2.2 Å resolution. *J. Mol. Biol.* 204, 191–204.
- (38) Lau, S. Y., Procko, E., and Gaudet, R. (2012) Distinct properties of Ca²⁺-calmodulin binding to N- and C-terminal regulatory regions of the TRPV1 channel. *The Journal of General Physiology* 140, 541–555.
- (39) Muskett, F. W., Frenkiel, T. A., Feeney, J., Freedman, R. B., Carr, M. D., and Williamson, R. A. (1998) High resolution structure of the N-terminal domain of tissue inhibitor of metalloproteinases-2 and characterization of its interaction site with matrix metalloproteinase-3. *J. Biol. Chem.* 273, 21736–21743.
- (40) Nilius, B., Prenen, J., Hoenderop, J. G. J., Vennekens, R., Hoefs, S., Weidema, A. F., Droogmans, G., and Bindels, R. J. M. (2002) Fast and Slow Inactivation Kinetics of the Ca²⁺ Channels ECaC1 and ECaC2 (TRPV5 and TRPV6). Role

Of The Intracellular Loop Located Between Transmembrane Segments 2 And 3.
Journal of Biological Chemistry 277, 30852–30858.

- (41) Persechini, A., and Cronk, B. (1999) The relationship between the free concentrations of Ca²⁺ and Ca²⁺-calmodulin in intact cells. *J. Biol. Chem.* 274, 6827–6830.
- (42) Erickson, M. G., Alseikhan, B. A., Peterson, B. Z., and Yue, D. T. (2001) Preassociation of calmodulin with voltage-gated Ca²⁺ channels revealed by FRET in single living cells. *Neuron* 31, 973–985.
- (43) Rodríguez-Castañeda, F., Maestre-Martínez, M., Coudevylle, N., Dimova, K., Junge, H., Lipstein, N., Lee, D., Becker, S., Brose, N., Jahn, O., Carlomagno, T., and Griesinger, C. (2010) Modular architecture of Munc13/calmodulin complexes: dual regulation by Ca²⁺ and possible function in short-term synaptic plasticity. *Embo Journal* 29, 680–691.
- (44) Simonovic, M., Zhang, Z., Cianci, C. D., Steitz, T. A., and Morrow, J. S. (2006) Structure of the calmodulin alpha II-spectrin complex provides insight into the regulation of cell plasticity. *J. Biol. Chem.* 281, 34333–34340.
- (45) Vlach, J., Samal, A. B., and Saad, J. S. (2014) Solution Structure of Calmodulin Bound to the Binding Domain of the HIV-1 Matrix Protein. *J. Biol. Chem.* 289, 8697–8705.
- (46) Phelps, C. B., Wang, R. R., Choo, S. S., and Gaudet, R. (2009) Differential Regulation of TRPV1, TRPV3, and TRPV4 Sensitivity through a Conserved Binding Site on the Ankyrin Repeat Domain. *Journal of Biological Chemistry* 285, 731–740.
- (47) Yuan, T., and Vogel, H. J. (1998) Calcium-Calmodulin-induced Dimerization of the Carboxyl-terminal Domain from Petunia Glutamate Decarboxylase: A Novel Calmodulin-Peptide Interaction Motif. *Journal of Biological Chemistry* 273, 30328–30335.
- (48) Yap, K. L., Yuan, T., Mal, T. K., Vogel, H. J., and Ikura, M. (2003) Structural Basis for Simultaneous Binding of Two Carboxy-terminal Peptides of Plant Glutamate Decarboxylase to Calmodulin. *J. Mol. Biol.* 328, 193–204.
- (49) Liu, Y., Zheng, X., Mueller, G. A., Sobhany, M., DeRose, E. F., Zhang, Y., London, R. E., and Birnbaumer, L. (2012) Crystal Structure of Calmodulin Binding Domain of Orai1 in Complex with Ca²⁺*Calmodulin Displays a Unique

Binding Mode. *Journal of Biological Chemistry* 287, 43030–43041.

- (50) Reichow, S. L., Clemens, D. M., Freitas, J. A., Németh-Cahalan, K. L., Heyden, M., Tobias, D. J., Hall, J. E., and Gonen, T. (2013) Allosteric mechanism of water-channel gating by Ca²⁺–calmodulin. *Nat Struct Mol Biol* 20, 1085–1092.
- (51) Skinner, S.P., Fogh, R.H., Boucher, W., Ragan, T.J., Mureddu, L. and Vuister, G.W. (2016). CcpNmr AnalysisAssign: a flexible platform for integrated NMR analysis. *Journal of Biomolecular NMR* 66, 111–124.
- (52) Bokhovchuk, F.M., Bate, N., Kovalevskaya, N. Goult, B.T., Spronk, C.A.E.M., and Vuister, G.W. , (2018) *Biochemistry*, THIS ISSUE.

**A Novel Mechanism for Calmodulin Dependent Inactivation of Transient
Receptor Potential Vanilloid 6**

Supplementary Materials

Neil Bate, Rachel E. Caves[‡], Simon P. Skinner[†], Benjamin T. Goult[#], Jaswir Basran,
John S. Mitcheson & Geerten W. Vuister^{*}

Department of Molecular and Cell Biology, Leicester Institute of Structural and
Chemical Biology, University of Leicester, Henry Wellcome Building, Lancaster
Road, Leicester, LE1 9HN, United Kingdom

[‡]Present address:

School of Physiology, Pharmacology and Neuroscience. Faculty of Biomedical
Sciences, University of Bristol, University Walk, Bristol, BS8 1TD
United Kingdom

[†]Present address:

School of Molecular and Cellular Biology, Faculty of Biological Sciences & Astbury
Centre for Structural Molecular Biology, University of Leeds, Leeds, LS2 9JT, United
Kingdom

[#]Present address:

School of Biosciences, University of Kent, Canterbury, Kent, CT2 7NJ, United
Kingdom

^{*}Corresponding author (gv29@le.ac.uk)

running title: Calmodulin Dependent Inactivation of TRPV6

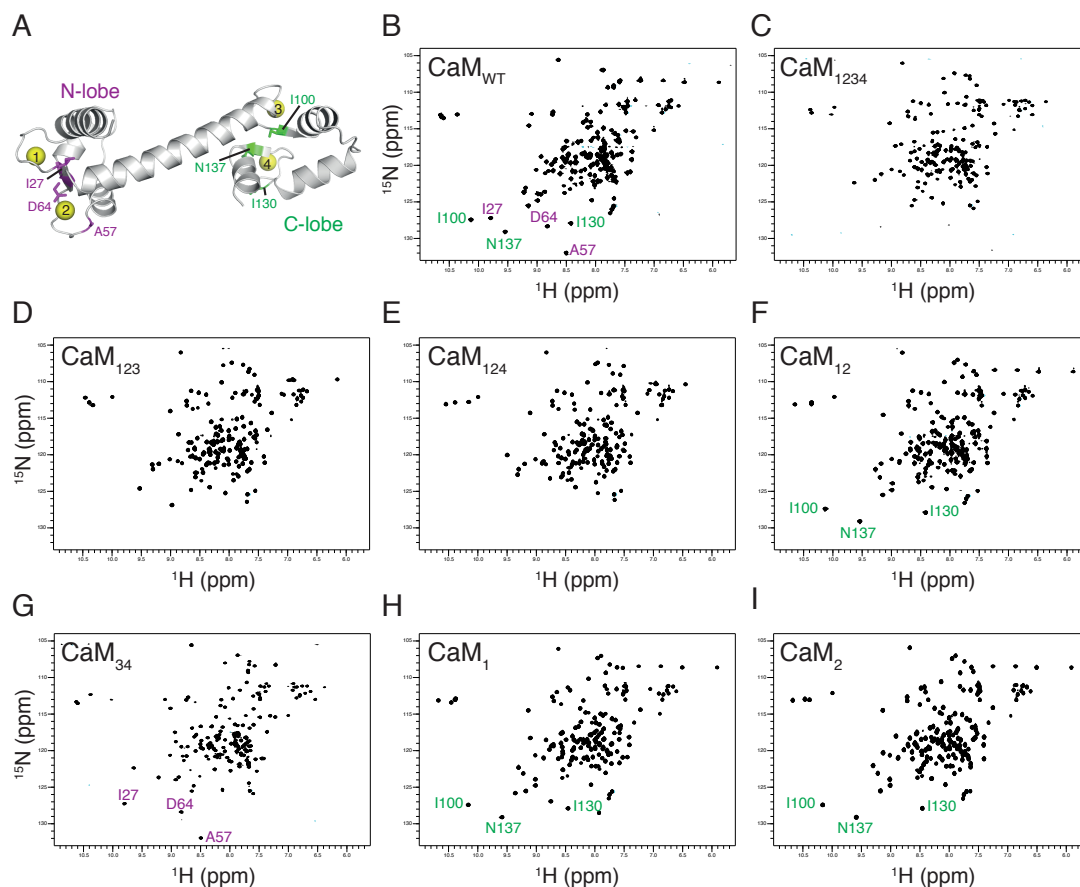


Figure S1- Evaluation of the CaM Ca²⁺-binding mutants.

A) Cartoon diagram of Ca²⁺-loaded CaM_{WT} (PDB:1CLL). Ca²⁺ ions are shown as yellow spheres and numbered following convention. Residues representative of the CaM_N and CaM_C lobes are shown in purple and green respectively.

B-I) ¹⁵N-¹H-HSQC spectrum of various Ca²⁺-loaded CaM mutants (Wu *et al*, 2012) displaying characteristic peaks of the CaM_N and CaM_C lobe residues in purple and green, respectively as highlighted in A).

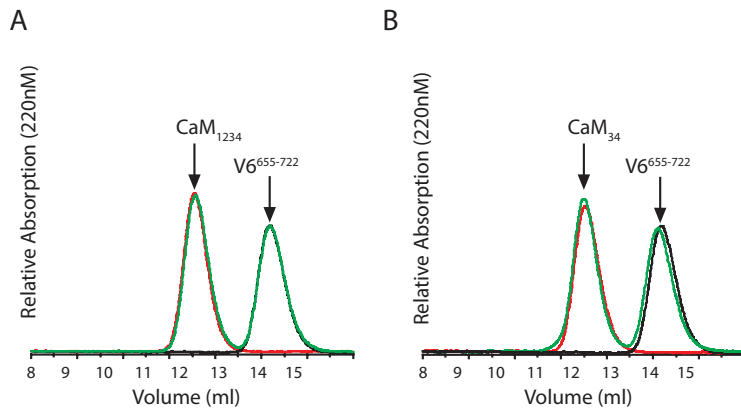


Figure S2- Analysis of TRPV6 C-tail binding to purified Calmodulin mutants; CaM₁₂₃₄ (A) and CaM₃₄ (B). Analytical gel filtration curves are displayed for each as follows; free TRPV6⁶⁵⁵⁻⁷²² in black, free CaM variants in red and the corresponding CaM:TRPV6⁶⁵⁵⁻⁷²² complexes at a 1:1 molar ratio in green.

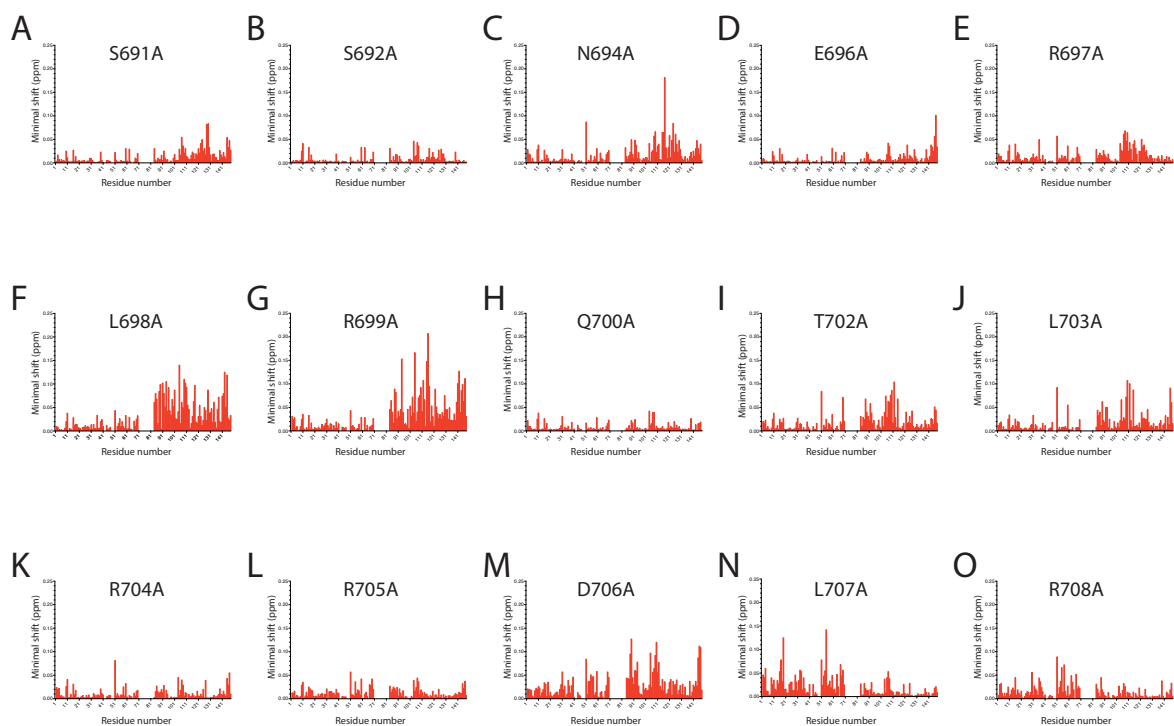


Figure S3- Mutagenesis of the TRPV6 C-tail Calmodulin (CaM_{WT}) binding site.

A-O) Alanine scanning mutagenesis of the TRPV6⁶⁵⁵⁻⁷²² C-tail CaM binding site. ¹⁵N-labelled CaM:mutant TRPV6⁶⁵⁵⁻⁷²² 1:1 complexes were analysed by ¹⁵N-¹H-HSQC NMR. Minimal shift CSPs ($\delta_{\text{bound mutants}} - \delta_{\text{bound}}$) as a function of residue were calculated as described in the materials and methods.

Reference

Wu P-R, Kuo C-C, Yet S-F, Liou J-Y, Wu KK & Chen P-F (2012) Lobe-Specific Calcium Binding in Calmodulin Regulates Endothelial Nitric Oxide Synthase Activation. *PLoS ONE* **7**: e39851